Supporting Information

Unlocking Zn Storage Performance of Ammonium Vanadate Nanoflowers as High-Capacity Cathodes for Aqueous Zinc-ion Batteries via Potassium Ion and Ethylene Glycol Co-Intercalation Engineering

Ji Chen[a,#], Xiaoyue Zhang[b,#], Yangjie Li[a], Xiaoying Li[a], Xiaoqin Zhang[a], Yuxiang Chen[a], Qiaoji Zheng[a], Xingqiao Wu[b], Heng Zhang[c,*], Xin Tan[b,*], Dunmin Lin[a,*]

[a]College of Chemistry and Materials Science, Sichuan Normal University, Chengdu 610066, China

[b]Institute for Carbon Neutralization Technology， College of Chemistry and Materials Engineering, Wenzhou University, Wenzhou.

[c]School of Materials Science and Engineering, Suzhou University of Science and Technology, Suzhou 215009, China.

Experimental

[#]These authors contributed equally

[*]Corresponding authors: Email: zhangheng@usts.edu.cn (Heng Zhang); xintan@wzu.edu.cn (Xin Tan); ddmd222@sicnu.edu.cn (Dunmin Lin); Fax: +86 28 84760802; Tel: +86 28 84760802

Chemicals: The compounds used included ammonium metavanadate (NH_4VO_3, Aladdin Biochemical Technology Co., Ltd., >99%), oxalic acid dihydrate ($H_2C_2O_4·H_2O$, Sinopharm Chemical Reagent Co., Ltd., >99%), ethylene glycol (CH_6O_2, Aladdin Biochemical Technology Co., Ltd., >99%) and potassium sulfate (Shanghai Aladdin Biochemical Technology Co., Ltd., >99%). All the chemicals were used as received without further purification.

Synthesis of K-NVO: The K-intercalated $NH_4V_4O_{10}$ was synthesized by a simple one-step hydrothermal reaction. In a typical synthesis, 0.354 g NH_4VO_3 was added to 60 ml of distilled water and stirred for 1 h until completely dissolved. Then, 0.2835 g of $H_2C_2O_4·2H_2O$ was added to the solution, and stirred until completely dissolved, and then 0.15 mmol of potassium sulfate was added. After that, the whole solution was transferred to a 100 mL PTFE-lined stainless-steel autoclave for a 24-hour reaction at 180 °C. The powders were collected by centrifugation and washed 3 times with distilled water and absolute ethanol, and dried overnight in a vacuum oven at 60 °C.

Synthesis of EG-NVO: The EG-intercalated $NH_4V_4O_{10}$ was synthesized by a simple one-step hydrothermal reaction. In a typical synthesis, 0.354 g $NH_4V_3O_8$ was added to 60 ml of distilled water and stirred for 1 h until completely dissolved. Then, 0.2835g of $H_2C_2O_4·2H_2O$ was added to the solution, and stirred until completely dissolved, and then 5 ml of ethylene glycol solution was added. After that, the whole solution was transferred to a 100 mL PTFE-lined stainless-steel autoclave for a 24-hour reaction at

180 °C. The powders were collected by centrifugation and washed 3 times with distilled water and absolute ethanol, and dried overnight in a vacuum oven at 60 °C.

Synthesis of K,EG-NVO: The K,EG-intercalated $NH_4V_4O_{10}$ was synthesized by a simple one-step hydrothermal reaction. In typical synthesis, 0.354 g NH_4VO_3 was added to 60 ml of distilled water and stirred for 1 h until completely dissolved. Then, 0.2835 g of $H_2C_2O_4 \cdot 2H_2O$ was added to the solution, and stirred until completely dissolved, and then 0.15 mmol of potassium sulfate and 5 ml of ethylene glycol solution were added. After that, the whole solution was transferred to a 100 mL PTFE-lined stainless-steel autoclave for a 24-hour reaction at 180 °C. The powders were collected by centrifugation and washed 3 times with distilled water and absolute ethanol, and dried overnight in a vacuum oven at 60 °C.

Synthesis of NVO: The synthesis procedure of $NH_4V_4O_{10}$ was similar to that of K-NVO, except the removal of K^+.

Material Characterizations: The crystal structure of the samples was characterized by X-ray diffraction (XRD, Miniflex, Rigaku with Cu Kα). The micromorphology of the samples was observed by scanning electron microscopy (SEM, zeiss/sigma500). The transmission electron microscopy (TEM) and the high-resolution transmission electron microscopy (HRTEM) images were obtained using a transmission electron microscope (JEOL JEM-2100 F). The chemical compositions and bonds of the materials were

determined by X-ray photoelectron spectroscopy (XPS, Thermo Scientific K-Alpha+). Fourier-transform infrared (FT-IR) spectroscopy measurements were carried out by Bruker Vertex 70 spectrometer. Raman spectra were collected with a Renishaw in a spectrometer. Electron Paramagnetic Resonance (EPR) spectra were collected by a Bruker A300 EPR Spectrometer. Contact angles were carried out by Shanghai Xuanzhun SZ-CAMC32. Ultraviolet photoelectron spectroscopy (UPS) spectra were collected by Thermo Fisher Scientific Nexsa.

Electrochemical Tests: Electrochemical measurements were performed on CR2032-type coin cells. The working electrode was prepared by mixing electrode, acetylene black and polyvinylidene difluoride (PVDF) in an N-methyl-pyrrolidone solvent at a ratio of 7:2:1 wt % and the slurry was coated on a titanium foil. The electrode was dried at 70℃ in a vacuum oven overnight. The mass loading of the cathode material was ~ 1 mg cm^{-2}. A glass fiber (Whatman, GF/D) and 2.0 M $Zn(CF_3SO_3)_2$ were utilized as the separator and electrolyte, respectively. The galvanostatic intermittent titration technique (GITT) and the Galvanostatic charge-discharge tests were carried out utilizing an automatic battery tester (LAND, CT2100A, China) in the voltage range of 0.3−1.6 V (vs Zn^{2+}/Zn). Cyclic voltammetry (CV) was conducted on an electrochemical workstation (CHI760E, China).

Measurements of Galvanostatic Intermittent Titration Technique (GITT)

The GITT test was performed at 0.1 A g^{-1}, which consisted of 5 min galvanostatic

charge (pulse) followed by a relaxation time of 10 min. The obtained GITT curves can be used to determine the zinc ion diffusion coefficients based on the following equation:

$$D = \frac{4L^2}{\pi\tau}\left(\frac{\Delta E_S}{\Delta E_t}\right)^2 \quad \text{(S1)}$$

where D is the diffusion coefficient, L is the diffusion length of Zn^{2+}, corresponding to the thickness of the electrode, τ represents the duration of current relaxation time, and ΔEs and ΔEt correspond to the steady-state potential change by the current pulse and voltage change under the constant current pulse, respectively. The ΔE_s and ΔE_t can be read and calculated by the LAND automatic battery tester.

Computational Methods

All of the spin-polarized density functional theory (DFT) calculations were carried out under the Device Studio platform using a first-principles calculations software (DS-PAW) [1], which uses the plane wave basis and the projector augmented wave (PAW) [2-4] for the treatment of core electrons. The Perdew, Burke, and Ernzerhof exchange-correlation functional within a generalized gradient approximation (GGA-PBE) [5] was used in our calculation and added van der Waals (vdW) correction. A supercell ($N_6H_{24}V_{24}O_{60}$) was constructed to model $NH_4V_4O_{10}$, with the introduction of potassium atoms and $C_2H_6O_2$ molecules to create three intercalation-modified models. In all calculations, a kinetic energy cutoff of 500 eV was adopted, and the Brillouin zone integration was performed on the (3×3×4) Monkhorst–Pack k-point mesh. The DFT+U method was employed to correct the localized 3d electrons of V with a U of 4.0 eV[6]. During geometry optimizations, all the structures were relaxed until the residual atomic

forces were less than 0.02 eV/Å, ensuring convergence of the total energy to 10−6 eV. The ionic convergence criterion for the force on each image during NEB calculations was set to 0.05 eV/Å.

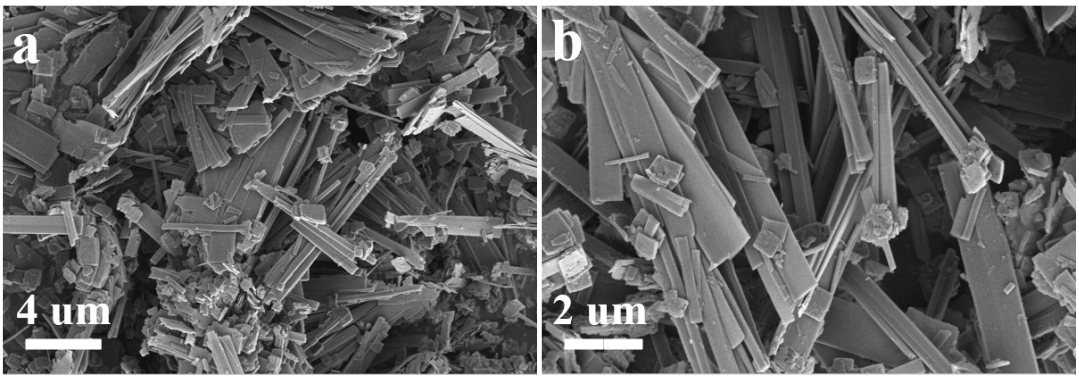

Figure S1. (a, b) SEM images of NVO.

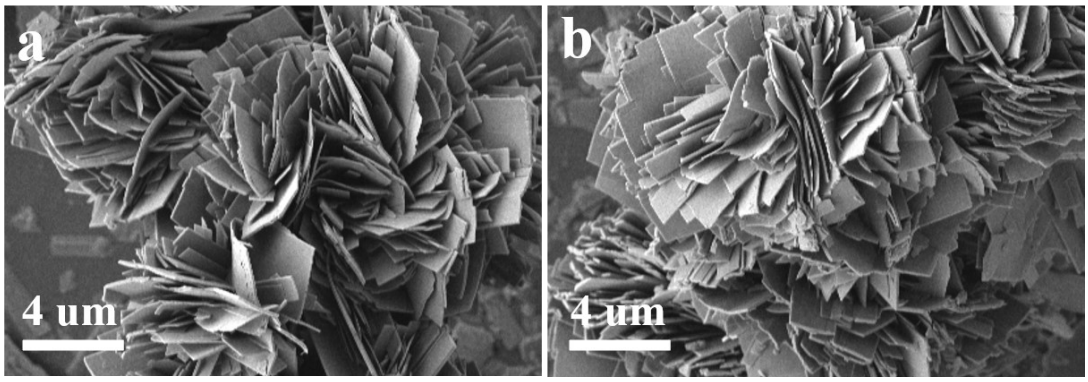

Figure S2. (a, b) SEM images of K-NVO.

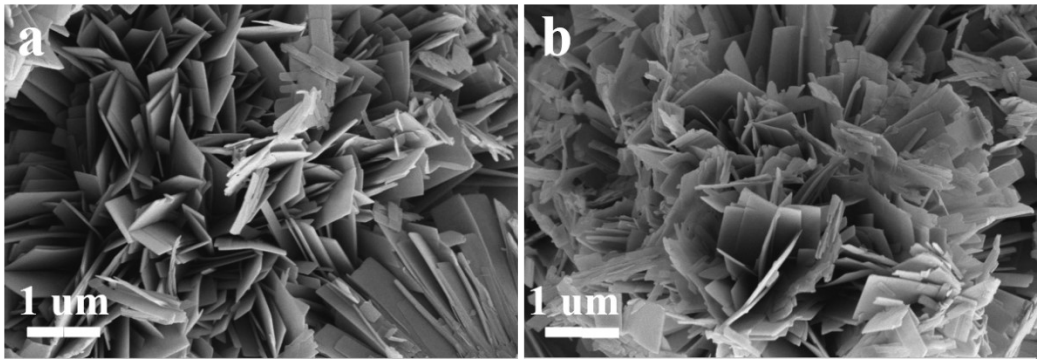

Figure S3. (a, b) SEM images of EG-NVO.

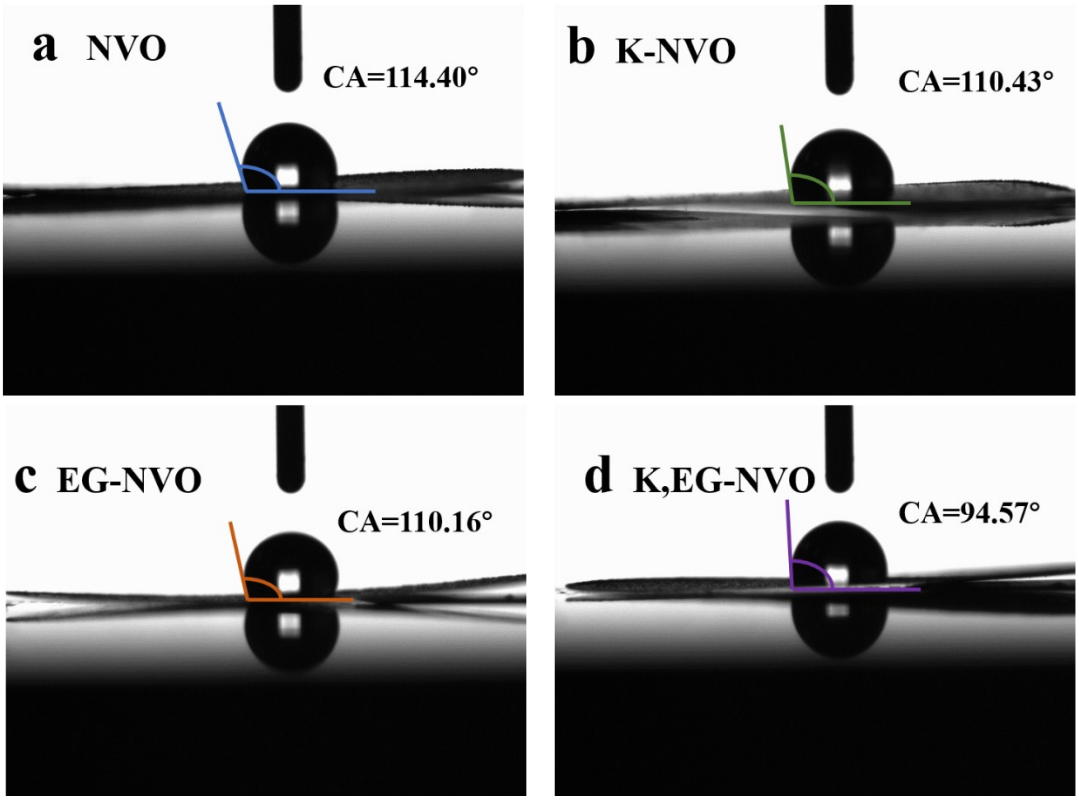

Figure S4. Contact angle of electrolyte with (a) NVO, (b) K-NVO, (c) EG-NVO and (d) K, EG-NVO electrode

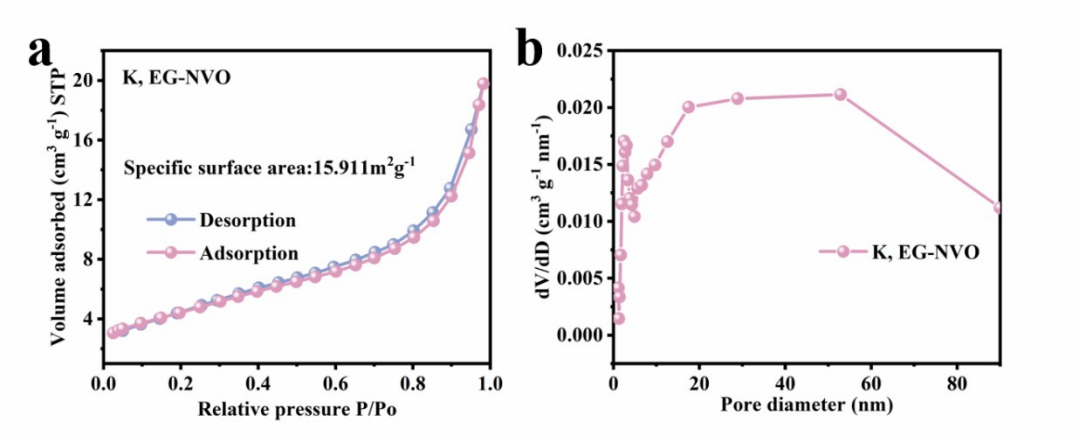

Figure S5. (a) N_2 adsorption/desorption isotherm, and (b) the corresponding pore size distribution of K, EG-NVO.

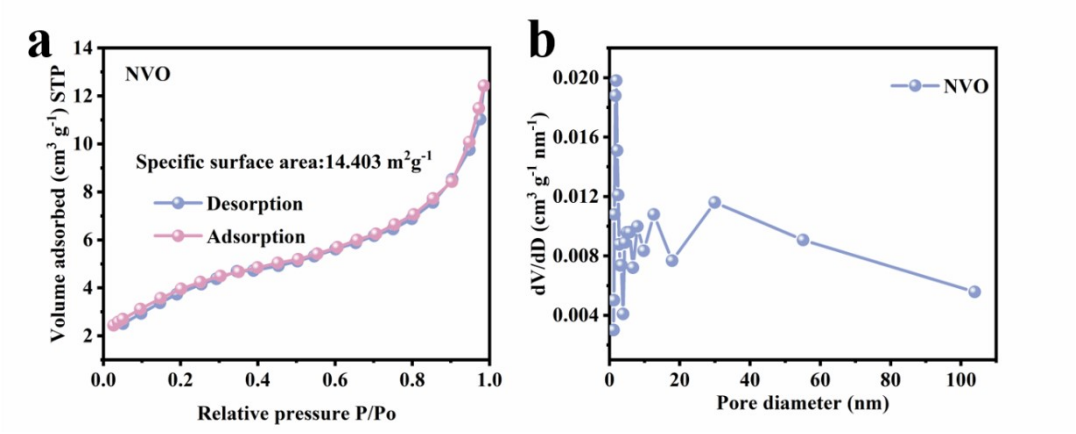

Figure S6. (a) N_2 adsorption/desorption isotherm, and (b) the corresponding pore size distribution of NVO.

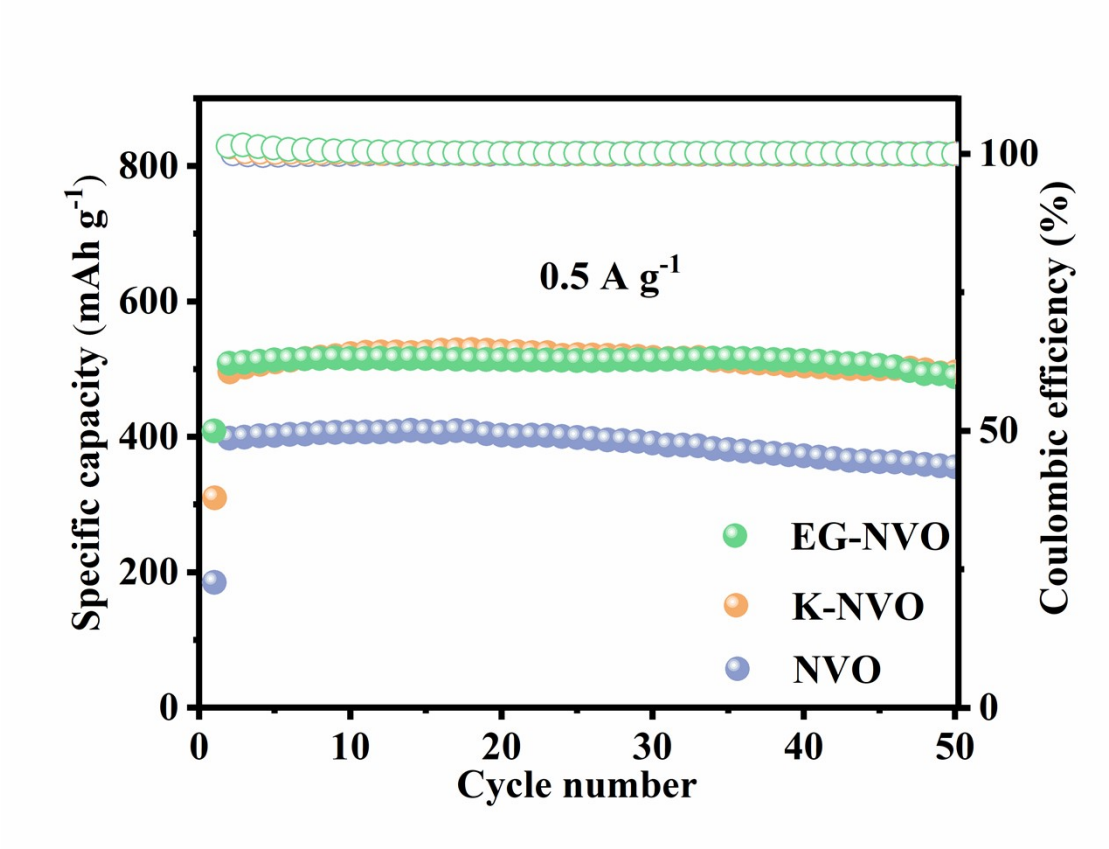

Figure S7. Cycling performance of NVO, K-NVO and EG-NVO at 0.5 A g^{-1}.

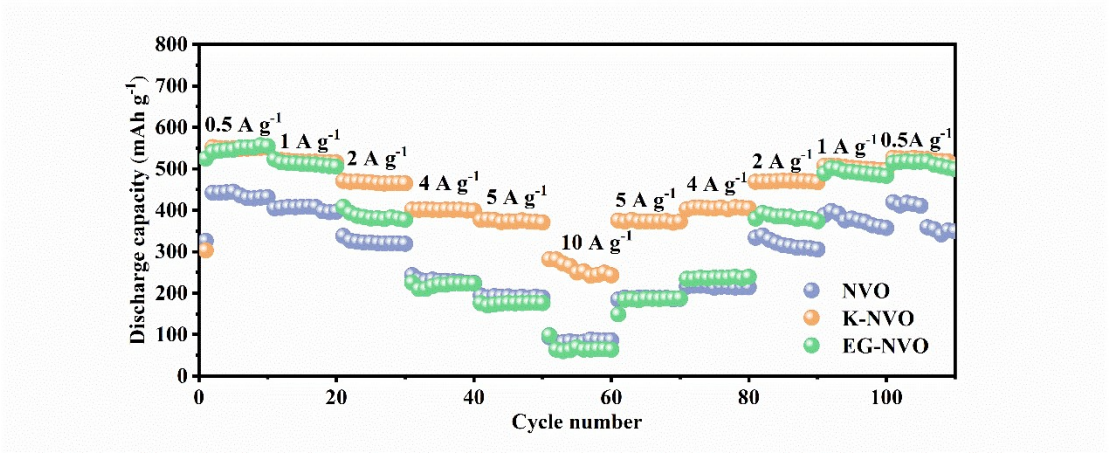

Figure S8. Rate performance of NVO, K-NVO and EG-NVO electrodes.

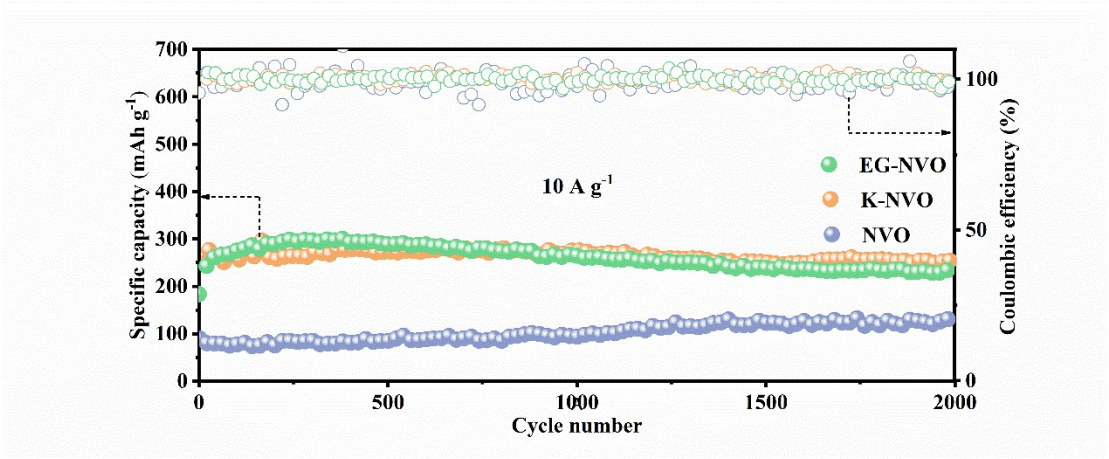

Figure S9. Cycling performance of NVO, K-NVO and EG-NVO at 10 A g^{-1}.

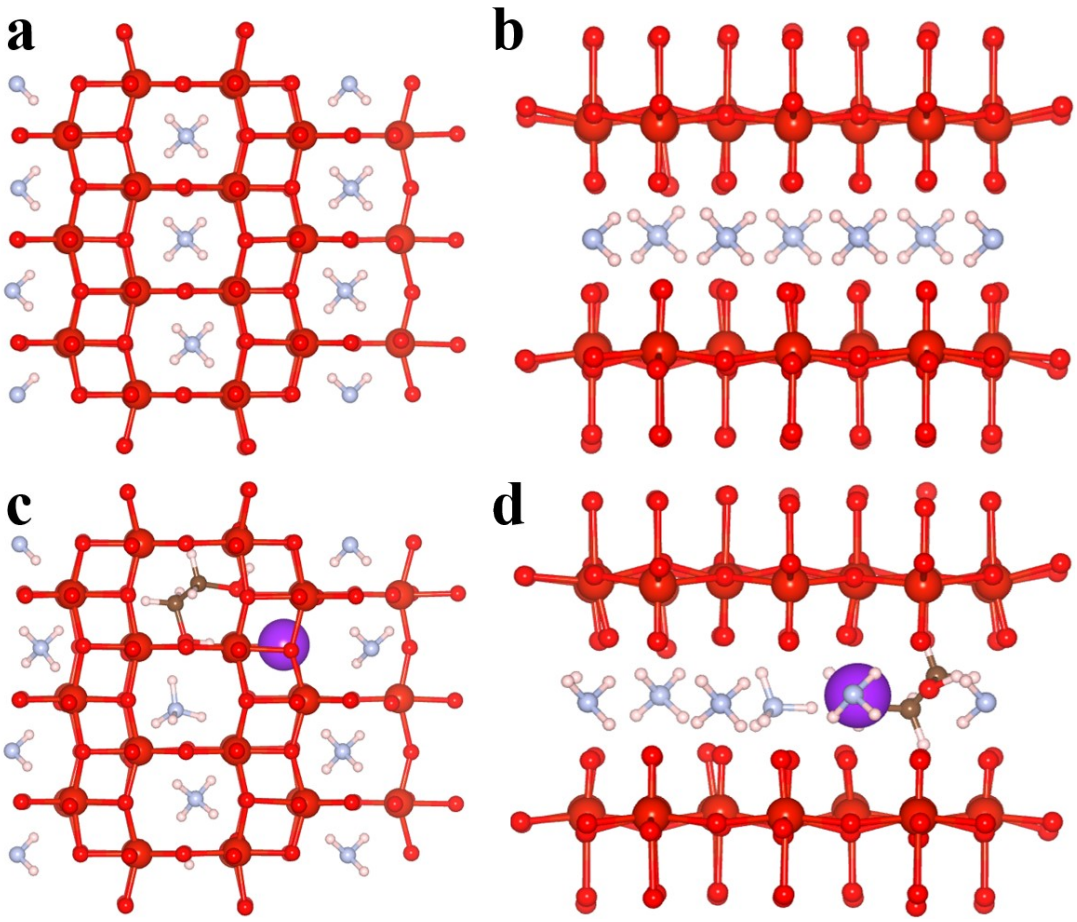

Figure S10. Geometric structures of (a, b) NVO and (c, d) K, EG-NVO.

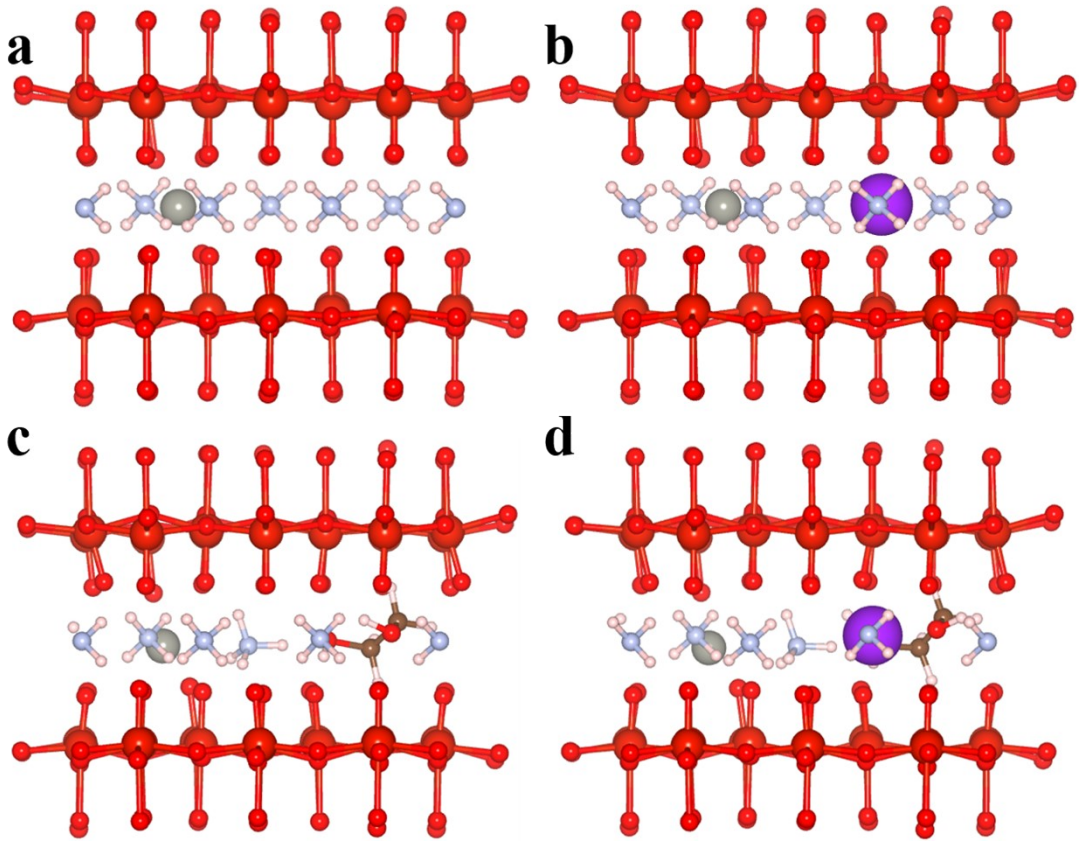

Figure S11. Geometric structures of (a) NVO, (b) K-NVO, (c) EG-NVO, and (d) K, EG-NVO with inserted zinc ions.

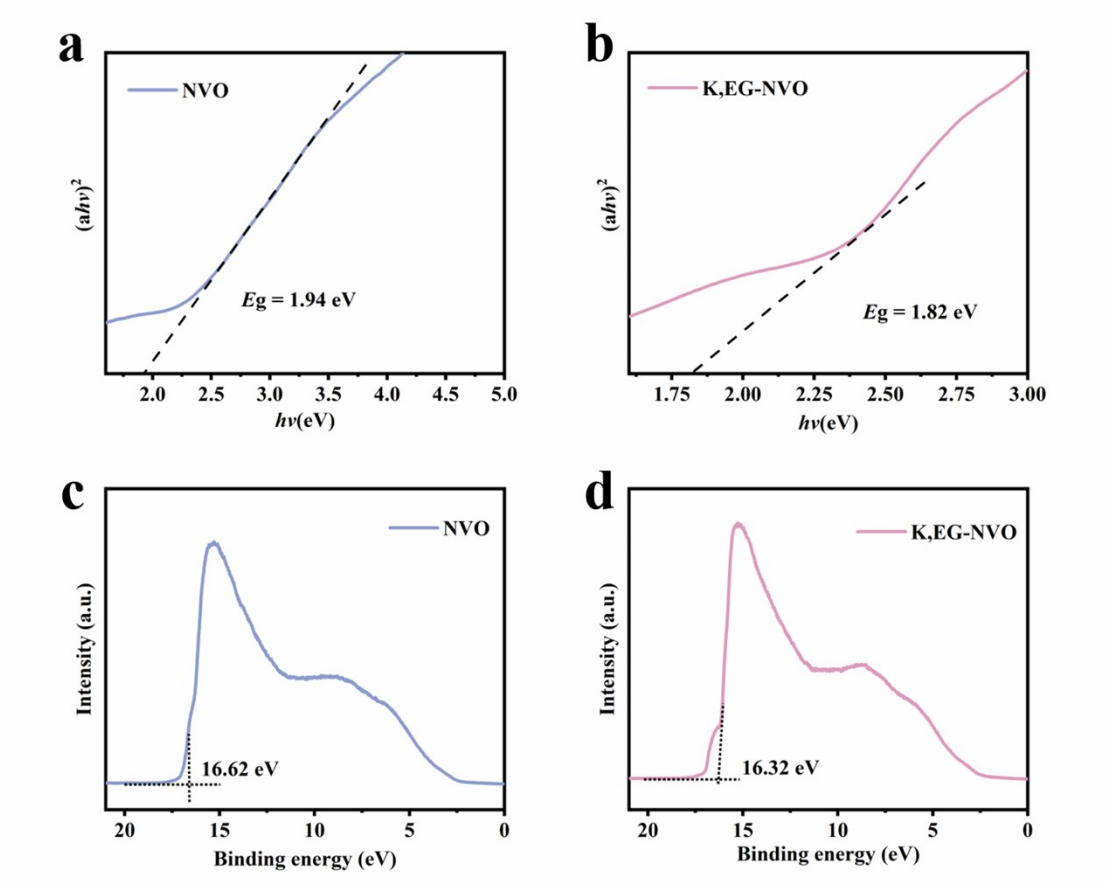

Figure S12. Tauc plots of UV-vis absorption spectra for (a) NVO and (b) K, EG-NVO; UPS spectra of (c) NVO and (d) K, EG-NVO.

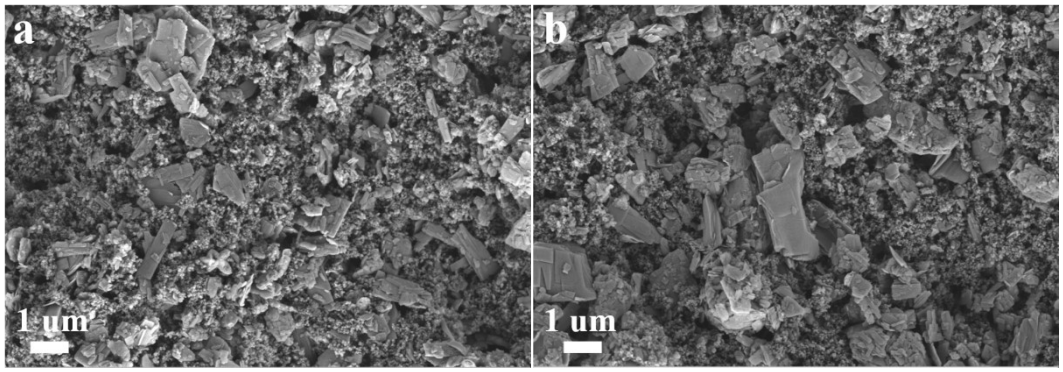

Figure S13. (a, b) SEM images of K, EG-NVO electrode before cycling.

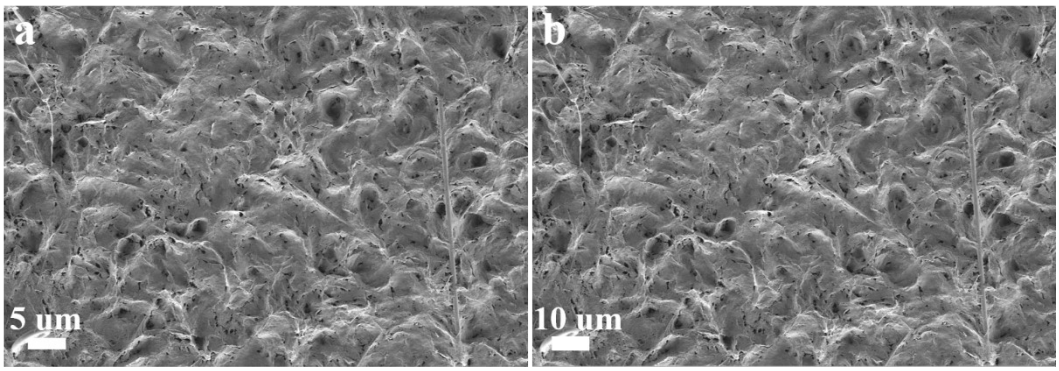

Figure S14. (a, b) SEM images of K, EG-NVO electrode discharged to 0.3 V for the first time.

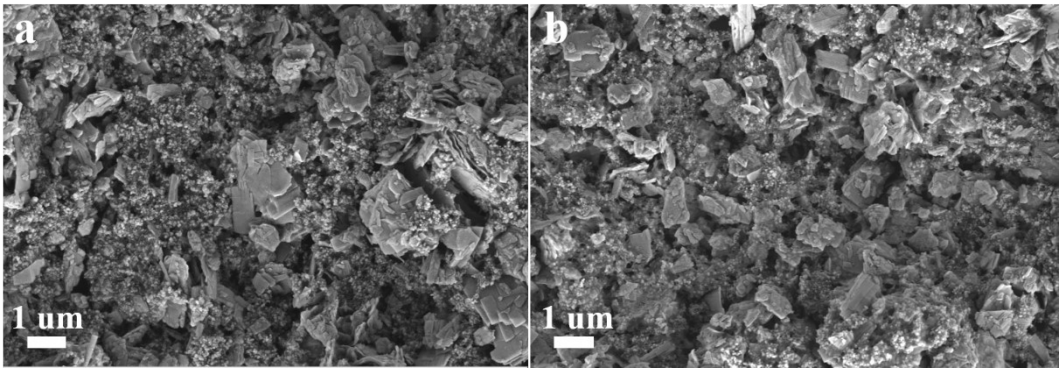

Figure S15. (a, b) SEM images of K, EG-NVO electrode charged to 1.6 V for the first time.

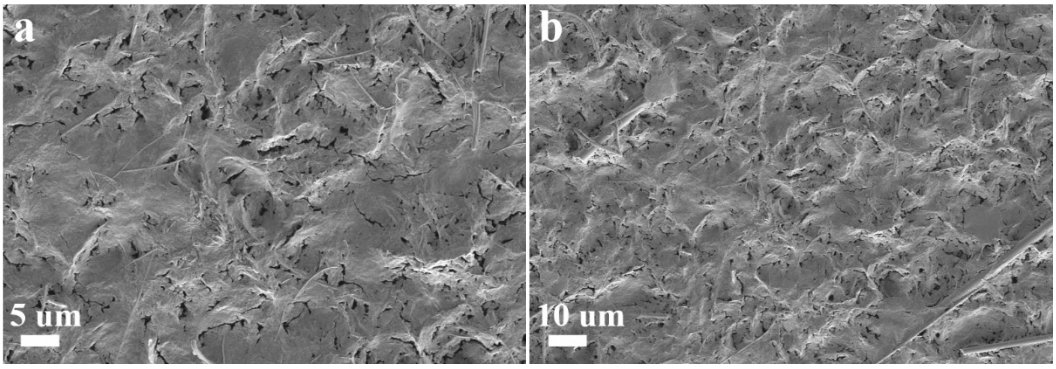

Figure S16. (a, b) SEM images of K, EG-NVO electrode at the 2nd discharge to 0.3 V.

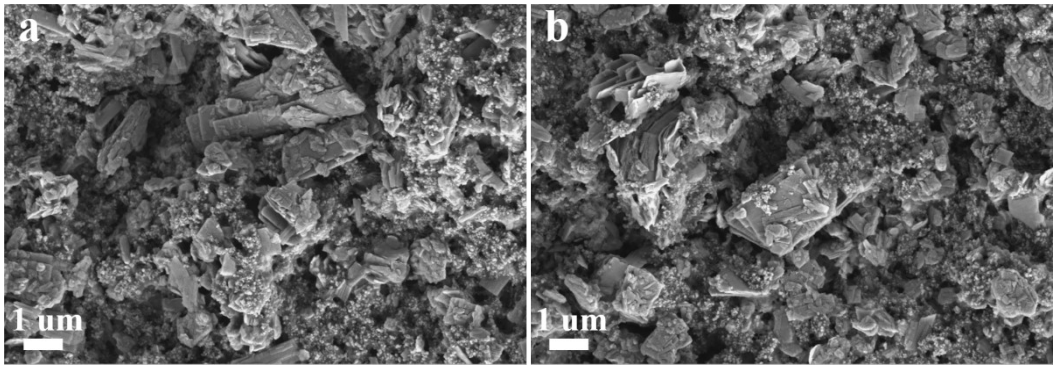

Figure S17. (a, b) SEM images of K, EG-NVO electrode at the 2nd charge to 1.6 V.

Table S1 Contents of K and V in K-NVO and K,EG-NVO samples by ICP.

Sample	Element	Elemental concentration (mg/kg)	Elemental concentration (mol/kg)	Chemical formula
K-NVO	V	5758390	112.9	$K_{0.18}NH_4V_4O_{10}$
	K	22079	5.09	
K,EG-NVO	V	5318520	104.3	EG-$K_{0.175}NH_4V_4O_{10}$
	K	19837	4.57	

Table S2. Composition of NVO-based samples with different amounts of structural water by thermogravimetric analysis.

Sample	Initial (ug)	100 ℃ (ug)	wt %
NVO	5310.85	5147.00	3.07%
K-NVO	5736.14	5570.89	2.89%
EG-NVO	5612.61	5224.17	6.91%
K, EG-NVO	5685.79	5446.37	4.2%

Table S3. Contents of EG in EG-NVO and K, EG-NVO samples by elemental analysis.

Sample	C (wt%)	EG (wt%)	N (wt%)	H (wt%)
EG-NVO	1.80%	4.65%	2.52%	1.38%
K, EG-NVO	0.35%	0.90%	1.83%	1.23%

Table S4. Comparison of electrochemical performance between this work and the state-of-the-art investigations on AZIBs.

Cathode	Voltage Window (V)	Electrolyte	Specific capacity	Ref.
Mg-$NH_4V_4O_{10}$	0.2-1.6	3 M $Zn(CF_3SO_3)_2$	410 mAh g^{-1} at 0.1 A g^{-1}	[7]
NaNVO-PANI	0.2-1.6	2 M $Zn(CF_3SO_3)_2$	617 mAh g^{-1} at 0.5 A g^{-1}	[8]
δ-$K_{0.49}V_2O_5$	0.3-1.5	3 M $Zn(CF_3SO_3)_2$	361 mAh g^{-1} at 0.2 A g^{-1}	[9]
(1Zn,1ch)-VOH	0.2-1.6	3 M $Zn(CF_3SO_3)_2$	424 mAh g^{-1} at 0.5 A g^{-1}	[10]
NiVO-BTA	0.3-1.4	3 M $Zn(CF_3SO_3)_2$	464.2 mAh g^{-1} at 0.2 A g^{-1}	[11]
CS@ZVO	0.3-1.7	3 M $Zn(CF_3SO_3)_2$	323 mAh g^{-1} at 0.1 A g^{-1}	[12]
α-V_2O_5@V_2CT_x	0.2-1.8	3 M $Zn(CF_3SO_3)_2$	595.2 mAh g^{-1} at 0.2 A g^{-1}	[13]
AVO	0.2-1.6	3 M $Zn(CF_3SO_3)_2$	427 mAh g^{-1} at 0.2 A g^{-1}	[14]
PEO-LVO	0.2-1.6	3 M $Zn(CF_3SO_3)_2$	438.1 mAh g^{-1} at 0.1 A g^{-1}	[15]
ZVO	0.3-1.6	3 M $Zn(CF_3SO_3)_2$	426.3 mAh g^{-1} at 0.2 A g^{-1}	[16]

K, EG-NVO	0.3-1.6	2 M $Zn(CF_3SO_3)_2$	604 mAh g^{-1} at 0.5 A g^{-1}	This work

References

[1] P.E. Blöchl, Projector augmented-wave method, *Phys. Rev. B*. 1994, ***50***, 17953-17979.

[2] G. Kresse, J. Furthmuller, Efficient iterative schemes for ab initio total-energy calculations using a plane-wave basis set, *Phys. Rev. B*. 1996, ***54***, 11169.

[3] G. Kresse, Furthmuller, J, Efficiency of ab-initio total energy calculations for metals and semiconductors using a plane-wave basis set Comput. *Mater. Sci*. 1996, ***6***, 15.

[4] G. Kresse, D. Joubert, From ultrasoft pseudopotentials to the projector augmented-wave method, *Phys. Rev. B*. 1999, ***59***, 1758-1775.

[5] J.P. Perdew, K. Burke, M. Ernzerhof, Generalized Gradient Approximation Made Simple, *Phys rev lett*. 1996, ***77***, 3865-3868.

[6] S.L. Dudarev, G.A. Botton, S.Y. Savrasov, C.J. Humphreys, A.P. Sutton, Electron-energy-loss spectra and the structural stability of nickel oxide: An LSDA1U study, *Phys. Rev. B.* 1998, ***57***, 1505.

[7] X. Wang, Y. Wang, A. Naveed, G. Li, H. Zhang, Y. Zhou, A. Dou, M. Su, Y. Liu, R. Guo, C.C. Li, Magnesium Ion Doping and Micro-Structural Engineering Assist $NH_4V_4O_{10}$ as a High-Performance Aqueous Zinc Ion Battery Cathode, *Adv. Funct. Mater.* 2023, ***33***, 2306205.

[8] S. Zhao, S. Wang, J. Guo, L. Li, C. Li, Y. Sun, P. Xue, D. Wu, L. Wei, Y. Wang,

Q. Zhang, Sodium-Ion and Polyaniline Co-Intercalation into Ammonium Vanadate Nanoarrays Induced Enlarged Interlayer Spacing as High-Capacity and Stable Cathodes for Flexible Aqueous Zinc-Ion Batteries, *Adv. Funct. Mater*. 2023, ***33***, 2305700.

[9] W. He, C. Meng, Z. Ai, D. Xu, S. Liu, Y. Shao, Y. Wu, X. Hao, Achieving fast ion diffusion in aqueous zinc-ion batteries by cathode reconstruction design, *Chem. Eng. J*. 2023, ***454***, 140260.

[10] Q. Zong, Y. Zhuang, C. Liu, Q. Kang, Y. Wu, J. Zhang, J. Wang, D. Tao, Q. Zhang, G. Cao, Dual Effects of Metal and Organic Ions Co-Intercalation Boosting the Kinetics and Stability of Hydrated Vanadate Cathodes for Aqueous Zinc-Ion Batteries, *Adv. Energy Mater*. 2023, ***13***, 2301480.

[11] J. Guo, J. Liu, W. Ma, Z. Sang, L. Yin, X. Zhang, H. Chen, J. Liang, D.a. Yang, Vanadium Oxide Intercalated with Conductive Metal–Organic Frameworks with Dual Energy-Storage Mechanism for High Capacity and High-Rate Capability Zn Ion Storage, *Adv. Funct. Mater*. 2023, ***33***, 2302659.

[12] J. Yang, J. Li, Y. Li, Z. Wang, L. Ma, W. Mai, M. Xu, L. Pan, Defect regulation in bimetallic oxide cathodes for significantly improving the performance of flexible aqueous Zn-ion batteries, *Chem. Eng. J*. 2023, ***468***, 143600.

[13] W. Wang, R. Hu, C. Zhang, Y. Tao, L. Ran, Y. Li, Y. Ouyang, J. Yan, A stepwise oxidation strategy for the synthesis of amorphous V_2O_5@V_2CT_x nanohybrid cathodes toward high-performance aqueous Zn-ion batteries, *J Mater Chem A*. 2023, ***11***, 8224-8234.

[14] W. Deng, Z. Xu, G. Li, X. Wang, Self-Transformation Strategy Toward Vanadium Dioxide Cathode For Advanced Aqueous Zinc Batteries, *Small* 2023, ***19***, 2207754.

[15] M. Wu, C. Shi, J. Yang, Y. Zong, Y. Chen, Z. Ren, Y. Zhao, Z. Li, W. Zhang, L. Wang, X. Huang, W. Wen, X. Li, X. Ning, X. Ren, D. Zhu, The LiV_3O_8 Superlattice Cathode with Optimized Zinc Ion Insertion Chemistry for High Mass-Loading Aqueous Zinc-Ion Batteries, Adv Mater 2024.

[16] L. Wang, K.-W. Huang, J. Chen, J. Zheng, Ultralong cycle stability of aqueous zinc-ion batteries with zinc vanadium oxide cathodes, *Sci Adv*. 2019, ***5***, eaax4279.